Materials Research Bulletin 142 (2021) 111421

Contents lists available at ScienceDirect

Materials Research Bulletin

journal homepage: www.elsevier.com/locate/matresbu

Role of substrate architecture and modelling on photocurrent and photovoltage in TiO_2/NiO transparent photovoltaic

Naveen Kumar[a,b], Nguyen Thanh Tai[a,b], Hyeong-Ho Park[c,*], Lee Kibum[d], Kim Sang Moon[e,*], Kim Joondong[a,b,*]

[a] Photoelectric and Energy Device Application Lab (PEDAL) and Multidisciplinary Core Institute for Future Energies (MCIFE), Incheon National University, Incheon 22012, South Korea
[b] Department of Electrical Engineering, Incheon National University, 119 Academy Rd. Yeonsu, Incheon 22012, South Korea
[c] Nanodevices Lab., Device Technology Division, Korea Advanced Nanofab Center (KANC), 109 Gwanggyo-ro, Yeongtong-gu, Suwon 16229, South Korea
[d] SolarLight Ltd., Incheon National University, 119 Academy Rd. Yeonsu, Incheon 22012, South Korea
[e] Department of Mechanical Engineering, Incheon National University, 119 Academy Rd. Yeonsu, Incheon 22012, South Korea

ARTICLE INFO

Keywords:
Enhanced photocarriers
Focusing light
Transparent photovoltaic (TPV)
ITO nanodome
Space charge region

ABSTRACT

A novel approach of focusing the incident light to enhance the photocurrent and photovoltage in TiO_2/NiO heterojunction-based transparent photovoltaics is deployed in this work. An ITO nanodomes periodic structure was used as a substrate to focus the incident light to the space charge region. The ITO nanodomes based device exhibited high optical transparency of ~60% in the visible-NIR region making it a better transparent photovoltaic. The modeling of the device was done by calculating the focal length of nanodomes. The approach was to simply overlap the photo-carrier generation region and space charge region for better charge collection efficiency. A significant improvement in the photocurrent (595.51±93.06 μA) and photovoltage (317.25±58.98 mV) was observed in the ITO nanodomes based TiO_2/NiO device. The ITO nanodomes based device also demonstrated spectral selective photodetection behavior with high responsivity (28±2 mA/W) and high response speed (<0.5 ms). This work fosters a novel approach to design photovoltaics of enhanced performance.

Introduction

Voracious usage of fossil fuels has rendered the gleaning of electrical energy from solar radiation an utmost priority. To harvest solar energy efficiently, a photovoltaic cell is the device used which has myriad of applications in military defense, self-powered electronics, smart windows and transportation [1-6]. Due to its simple fabrication, ability to be grown on a large area, and direct extraction of produced electrical energy it is commercialized and found its niche in solar energy harvesting [7–10]. Though, the progressive enhancement in the performance of photovoltaic has been an open topic for research and commercialization [9–12]. Despite a progressive enhancement in the performance of traditional photovoltaics, they still lack in the many application domains such as in transparent electronics, transparent window, and in transparent roof. Their limitation is mainly attributed to their low band gap, which make them opaque. Hence, in last few years enormous attention is given to the development of transparent photovoltaic (TPV) which combine high optical transparency with solar energy conversion [13]. Forty percent of energy produced in the worlds is consumed by the buildings, and this percentage is expected to increase more in the future [14] . Transparent photovoltaics provides the solution by demonstrating the ease of being integrated in the buildings, transports, and in electronic devices without compromising the aesthetics and transparency of the buildings or devices. Yet a significant attention is given to the traditional photovoltaics by adopting several approaches that improve photovoltaic parameters like open-circuit voltage (V_{OC}), short-circuit current (I_{SC}), fill factor (FF), and the dark current (I_o) forsaking TPVs [15]. Though TPVs offer high optical transparency in the visible-NIR region, yet their performance is limited by the low photovoltage and photocurrent [16].

The fundamental approaches that can be used to increase the photocurrent density in photovoltaics are to increase the optical path length of the incident light in the absorber layer and reduce the optical loss in the transparent conducting oxides. To do so in traditional photovoltaics, approaches such as interfaces/surfaces functionalization, surface texturing design schemes, decrease the free carrier absorption in

* Corresponding authors.
E-mail addresses: hyeongho.park@kanc.re.kr (H.-H. Park), ksm7852@inu.ac.kr (S.M. Kim), joonkim@inu.ac.kr (J. Kim).

https://doi.org/10.1016/j.materresbull.2021.111421
Received 29 March 2021; Received in revised form 20 May 2021; Accepted 21 May 2021
Available online 29 May 2021

the NIR region and increase the electrical mobility of transparent conducting oxides (TCOs) have been deployed to improve the photovoltaic performance [17–21]. The widely adopted approaches are the functionalization of the interfaces/surfaces and incorporating high carrier mobility and low carrier density TCOs in the photovoltaics due to their ease of incorporation in the heterojunction over the complexity of texturing formation of the surface [19, 20, 22–27].

The challenge of the surface modification readily causes the burdens of the additional steps, resulting in the complex in procedures with cost [28]. Direct etching of the absorber film may also lead to the formation of the surface defects and also affect the texture of the underneath films or requires the high accuracy in the surface texturing [29, 30]. The defects induced recombination is the main cause in deteriorating the electrical performance of the PVs [31]. On the other hand, TCOs suffer from low carrier mobility and high free carrier absorption in the NIR region. Therefore, in order to enhance the optoelectronic properties of TCOs, Parthiban et al., proposed Mo doped Indium Oxide as a transparent conducting oxides which showed a high mobility and low carrier density compared to the crystalline ITO thin films [20]. Similarly, many other reports have been found where a significant enhancement in carrier mobility of TCOs (H:ZnO, Al:ZnO, InZnO, GaZnO) is achieved [32–34]. Amidst different approaches, photonic and plasmonic have also demonstrated their potential in photovoltaics. Several reports are found where nanostructures such as nanosphere and nanorods were used to magnify and focus the light using the localized surface plasmon resonance [35–40]. Tediousness of making photonic structure and generation of heat due to plasmonic excitations in metal nanoparticles limit their potential and vivid usage in photovoltaics [41–43].

Many thin film TPVs such as a-Si, CdTe, polymer, and perovskite PVs were tuned to improve the performance and transparency [44–47]. Pavan et al., demonstrated very of its first kind of all oxide TiO_2/Cu_2O heterojunction transparent solar cell by spray pyrolysis. A detailed combinatorial approach is used to find the suitable thickness of Cu_2O to absorb the maximum photons [48]. Despite adopting various approaches, low transparency and limited power conversion efficiency have remained a long-standing challenge. Recently, TiO_2/NiO heterojunction TPVs have gained the huge interest due to their high optical transparency and stability, and optimum photovoltaics performance in the UV-NIR region [49, 50]. Nonetheless, in TiO_2/NiO TPVs, any interface/surface functionalization or surface modifications have not been deployed and very limited study has been done to improve the photovoltaic performance. Notwithstanding the approaches of interface/surface functionalization and surface texturing, the simplest approach is needed that can directly enhance the photo-carrier generation and photo-carrier collection efficiency without introducing surface defects and without making fabrication process tedious.

Therefore, in this work, a unique approach of ITO nanodomes for the periodic structure which is used as a substrate has been deployed to enhance the photocurrent and photovoltage in the TiO_2/NiO TPV offering high optical transparency compared to semiconductor-based PVs.

Here in this work, the ITO nanodomes substrate was used in such a way to focus the incident light over the space charge region (SCR) of TiO_2/NiO heterojunction that maintains high optical transparency. The thickness of different layers ITO, TiO_2, and NiO was kept in such a way that the ITO nanodomes can focuse the incident light at its focal point which is a SCR in the TiO_2/NiO heterojunction-based device. The SCR has the highest charge collection efficiency due to the strong electric field arisen inside the SCR region. Therefore, tuning the SCR in the light-absorbing entities or made the incident light focus over the SCR can be the approach to enhance the TPV performance. This work demonstrates the importance of substrate architecture and the simplest way to use nanostructure substrate to enhance the photocurrent and photovoltage by tuning and focusing the light over the SCR. The ITO nanodomes based device showed high transparency and high photovoltage than glass substrate based TiO_2/NiO TPV.

Experimental methods

Formation of ITO nanodome structure

We used a krypton-fluoride (KrF) stepper semiconductor process with a wavelength of 248 nm for the fabrication of ITO nanodomes structure on 6-inch ITO-coated glass wafer for industrial applications. This wafer-scale fabrication method of the ITO nanodomes has rapid, high-throughput and is highly reliable for the fabrication of TPV. To fabricate the ITO nanodomes on ITO-coated glass wafer, serial processes of KrF excimer laser lithography, ITO evaporation and lift-off were performed. Firstly, a lift-off resist (LOR) 5A (MicroChem Corp.) was spin-coated at 3000 rpm for 60 s on ITO-coated glass wafer and baked at 170 °C for 5 min. Then, a KrF photoresist (DJKI-2525, Dongjin Semichem. Corp.) was spin-coated at 2000 rpm for 60 s onto the LOR layer and baked on hot plate at 100 °C for 60 s. After exposure was conducted at a dose of 20 mJ/cm^2 using a KrF stepper (PASS 5500/300C, ASML), post-exposure baking was done at 110 °C for 60 s. Then, the resist film was developed with a 60 s immersion in a tetramethylammonium hydroxide (TMAH) solution. During the developing process, LOR hole-arrays were continuously achieved. We deposited a 200 nm-thick ITO film on the LOR hole-array glass substrate using an electron beam evaporation process. A lift-off process was performed to remove the LOR layer in a TMAH solution under 15 min of sonication; there remained a 200 nm-height ITO nanodomes (with a radius of 180 nm) array on the glass substrate, as presented in the top-view image (Fig. 1b) and in the cross-sectional view image (Fig. 1c and 1d).

Transparent photovoltaic cell fabrication

A glass substrate and ITO nanodomes based substrate was used to fabricate TiO_2 /NiO based TPV. The glass and ITO nanodomes substrates were cleaned in acetone, methanol, and deionized (DI) water by 10 min of ultra-sonication after each step and dried by N_2 flow before loading into the sputtering chamber. On the top of the glass substrate and ITO nanodomes substrate, the ITO thin film of thickness ~475 nm was deposited. The ITO was deposited at the DC sputtering power of 300 W, Ar flow of 30 sccm, and 5 mtorr of growth pressure. The reason of deposition 475 nm thick ITO on the top of glass and ITO nanodomes is discussed in the results and discussion section. The ITO layer was deposited back side of the ITO nanodome substrate so that ITO nanodomes remains at the opposite side. On the ITO nanodomes, a 40 nm ITO layer was also deposited to the minimize the reflection of the incident light under the quarter wavelength anti-reflection scheme using $d = \lambda/4n$. Where d, λ, and n are the thickness, wavelength of the incident light, and refractive index of the material (ITO).

On the ITO, the TiO_2 and NiO layers were grown. The TiO_2 layer was deposited by a two-step process, where the first step involved the deposition of the Ti layer by direct current (DC) sputtering and the second step was the oxidation of the Ti layer by rapid thermal annealing (RTA). A Ti sputtering target (iTASCO, 99.99% purity) was used for the deposition of the Ti layers. The Ti layer was deposited at 300 W under 5 mtorr deposition pressure. The Ar flow was maintained at 50 sccm. The deposition time for the Ti layer was 5 min to maintain the thickness of TiO_2 100 nm. The Ti layers were later oxidized by RTA in Ar and O_2 ambient at 500 °C for 15 min.

To deposit the NiO layer over TiO_2, a reactive sputtering method was used. A Ni sputtering target (iTASCO, 99.99% purity) was sputtered in Ar/O_2 ambient at 50 W. The deposition pressure was kept 3 m torr. The NiO layer thickness was ~20 nm. To maintain this uniformity, the substrate was rotated at 5 rpm. Prior to the deposition, the system was pumped down to the base pressure of 5×10^{-6} torr. To make the device completely transparent, silver nanowires (AgNWs, diameter ~20 nm and length ~20 μm, Nanopyrix), were spin-coated over the TiO_2/NiO heterojunction. The spin-coated films were dried at 100 °C for 2 min on a hot plate.

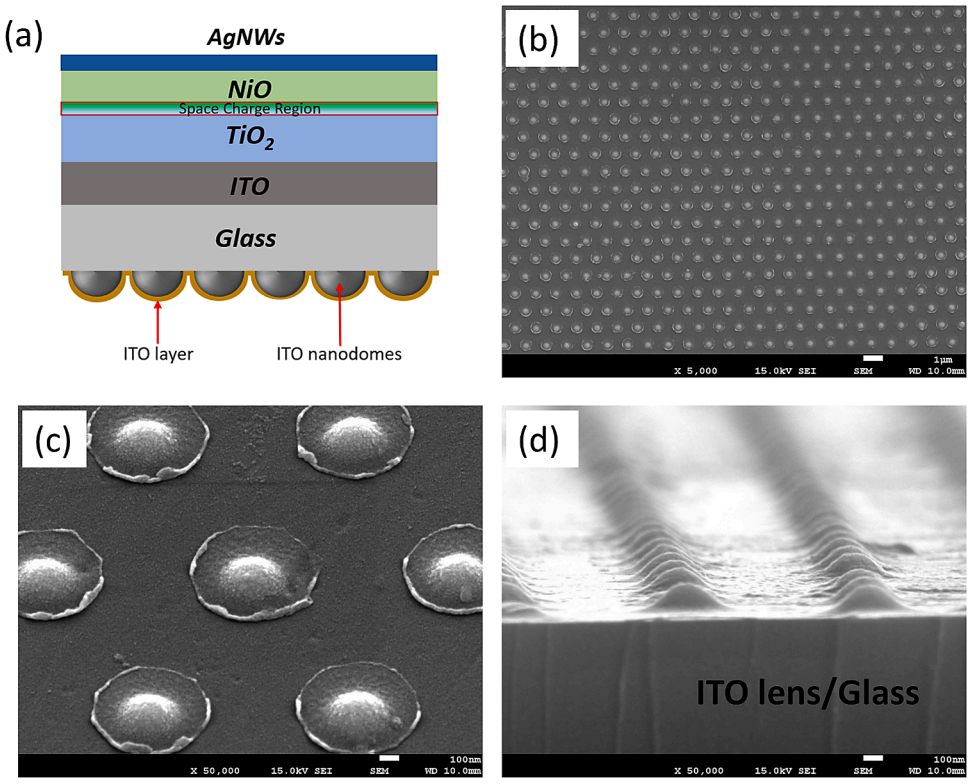

Fig. 1. (a) Schematic of the fabricated TiO_2/NiO transparent photovoltaic cells on the inverted ITO nanodomes substrate. (b) and (c) are the enlarge and zoomed-in FESEM image of ITO nanodomes structure. (d) Cross sectional FESEM image of ITO nanodomes substrate.

2.3. Characterizations

A field emission scanning electron microscope (FE-SEM, JEOL, JSM_7001F) was used to record the ITO nanodome structure and cross section image. The optical characteristics of samples were determined by transmittance plots obtained from a UV-visible-NIR spectrophotometer (Shimadzu, UV-2600). These spectra were obtained over a wavelength range of 300 to 1100 nm. A potentiostat/galvanostat (PGStat, WonA tech, Zive SP2) was used to characterize the device. Linear sweep voltammetry, with a scan rate of 100 mV/s, was applied to determine the I-V characteristics. Light-emitting diodes of wavelength 365 nm (LZ1-10UV00-0000) was used as light source. It was coupled to a dual-adjustable power supply (MCH-305DII) and a function generator (MFG-3013A, MCH Instruments). We used a solar power meter (KUSAM-MECO, KM-SPM-11) and UV light meter (Lutron, UV-340A) to calibrate the light sources with visible radiation. The active area of the device was defined by the contact area of the shadow mask.

Results and discussion

Structural and optical characterizations

A schematic diagram of the ITO nanodomes based TiO_2/NiO TPV is shown in Fig. 1(a). The ITO nanodomes substrate was inverted and the ITO film that was later used as a cathode (-Ve terminal) was grown on the backside of the ITO nanodomes substrate. The ITO nanodomes are nothing but periodically patterned ITO semi-nanosphere on the glass substrate. In order to make complete transparent photovoltaic, the TiO_2, NiO, and Ag Nanowires were deposited subsequently. To record the periodicity of ITO nanodomes, FESEM was performed over the ITO nanodomes substrate. Fig. 1(b) shows the enlarged view of the ITO nanodomes that shows the remarkably identical and periodically repeated ITO semi-nanosphere. These ITO semi-nanospheres were addressed as ITO nanodomes throughout the article. Fig. 1(c) is the zoomed-in view of the FESEM image of Fig. 1(b). Fig. 1(c) clearly shows the identicality and periodicity of the ITO nanosphere. Fig. 1(d) is the cross-sectional FESEM image of the ITO nanodomes on the glass. The cross-sectional FESEM image was used to calculate the height (h) and the radius (r) of the ITO nanodomes which was used to calculate the radius of the curvature (R) of ITO nanodomes using Eq. (1).

$$R = \frac{h^2 + r^2}{2h} \tag{1}$$

High optical transparency and a high performance are the essential demand for TPVs; therefore, the optical transparency was recorded by performing UV-visible photo-spectroscopy on the TiO_2/NiO heterojunctions. The optical transmittance spectrum of the TiO_2/NiO heterojunctions deposited on ITO nanodomes and the glass substrate, are shown in Fig. 1(a) and 1(b), respectively.

To have the comparison of ITO nanodomes based device, a TiO_2/NiO heterojunction-based TPV is also fabricated on the glass substrate at identical growth condition as used for ITO nanodomes based TPV. Both the devices showed high optical transparency. The high transparency of TiO_2/NiO TPV can be assigned to the wide bandgap of the TiO_2 and NiO layer. Both the devices showed high optical transparency of ~ 60 % in the visible NIR region. The high optical transparency offered by the devices can be attributed to the high band gap of ITO, TiO_2, and NiO. The little high optical transparency of the glass substrate-based TPV can be attributed to the large area-based device used for optical measurement. Another reason for showing comparatively low optical transmittance can be reflection offered by the ITO nanodomes during the optical measurements.

To confirm the structural phase of deposited TiO_2 and NiO thin films, XRD was performed and XRD profiles of TiO_2 and NiO are presented in Fig. 2(b) and 2(c), respectively. The observed peaks at 2θ of 27.4, 36.1, 41.3° correspond to the planes (110), (101), and (111), respectively, ensuring the formation of crystalline rutile phase of TiO_2 (JCPDS #88-1175). The XRD peaks at $2\theta > 50^o$ can be attributed to the Si substrate.

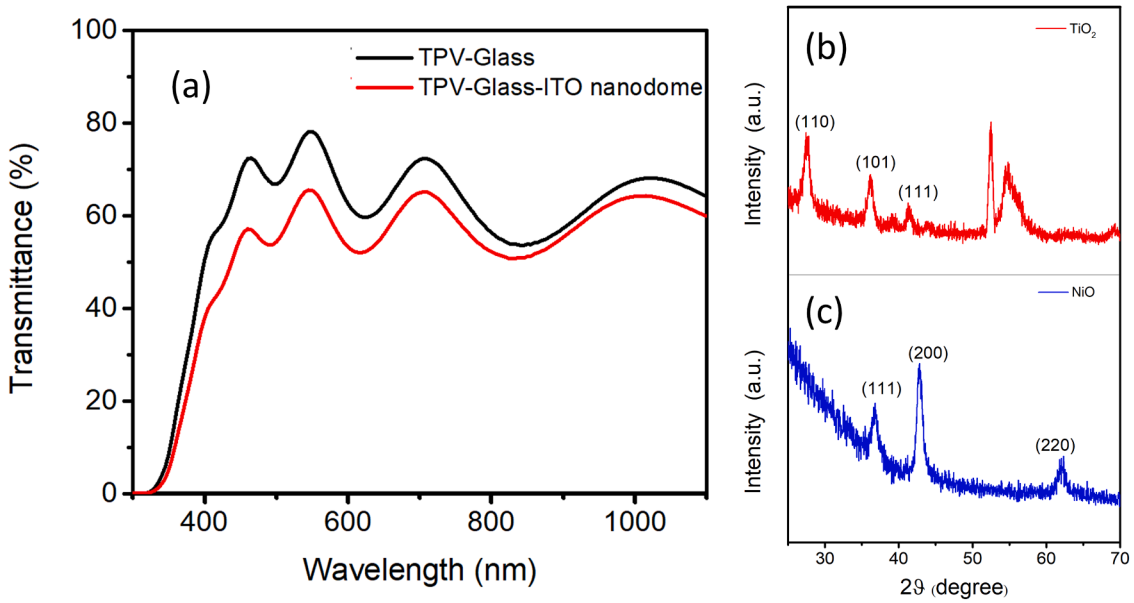

Fig. 2. (a) Optical transmittance of the TiO_2/NiO heterojunction-based TPV on the glass substrate and on the ITO nanodomes based substrate. XRD spectrum of (b) TiO_2 layer and (c) NiO layer.

Similarly, the XRD spectrum of NiO has shown peaks at 2θ of 36.8, 42.8, and 62.1° corresponds to the planes (111), (200), and (220), respectively. The obtained XRD peaks of NiO confirm the formation of crystalline NiO (JCPDS #471049).

I-V characterizations

Finally, to see the effect of substrate architecture on the device performance, the current-voltage (I-V) measurement was carried out on the TiO_2/NiO TPV grown on the glass substrate and ITO nanodomes substrate under dark and UV illumination. The intensity of the UV incident light was also varied from 1 to 20.1 mW/cm^2 to see the effect of light intensity on the photocurrent and photovoltage. Fig. 3(a) and 3(b) represent the semilog scale I-V behaviour of glass substrate-based TPV and ITO nanodomes substrate-based TPV, respectively. ITO nanodome based device showed clearly a distinctive and improved performance in the I-V properties. It was interesting to note that the glass-based device did not show any enhancement in the photocurrent and photovoltage under the illumination of the light of a wavelength of 365 nm of various intensities. On the contrary, the ITO nanodome based device showed an

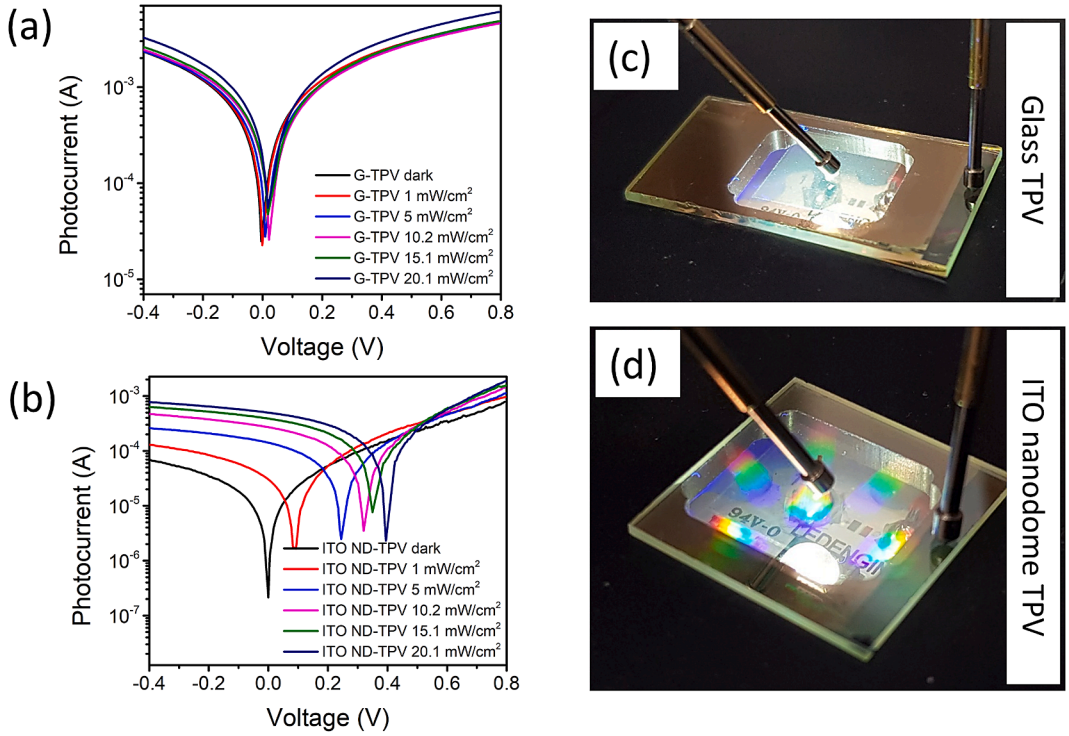

Fig. 3. (a) Semi-log scale plots of (a) glass based TiO_2/NiO TPV and (b) ITO nanodomes based TiO_2/NiO TPV. (c) Image of the glass-based TPV and (d) ITO nanodomes based TiO_2/NiO TPV.

order of significant enhancement in the photocurrent with the lowest dark current and photovoltage. The ITO nanodomes based TPV showed a high photocurrent and photovoltage of 595.51±93.06 μA and 317.25±58.98 mV, respectively, under the illumination of light source of wavelength 365 nm of power intensity of 20.1 mW/cm^2. On the contrary, the glass substrate-based TPV showed low photocurrent and photovoltage of 174.92±47.65 μA and 30.20±20.15 mV, respectively, under the illumination of light source of identical wavelength and intensity. Though the dark/photo current obtained in glass substrate-based TPV is higher than the ITO nanodome, yet the device is lacking in photocurrent and photovoltage enhancement. A poor variation in photocurrent and high dark current in glass substrate-based device may be due to poorly focusing of the incident light around/at the TiO_2/NiO space charge region and poor quality of heterojunction which may result in the inadequate generation of photo carriers [51]. High dark current is detrimental for photovoltaics and degrades the device performance noticeably [52]. The photocurrent is directly proportional to the power intensity of the illuminated light source and follows power law ($I\alpha P^{\alpha}$) [49, 53, 54]. Hence, a substantial increase in the photocurrent in ITO nanodomes based TPV with the increase in the intensity of illuminated light can be attributed to the generation of more photocarriers.

In the ITO nanodome based device, the Voc was improved up to 317.25±58.98 mV while it remained almost unchanged in the glass substrate-based TPV. The Fig. 3(c) and 3(b) show the images of glass TPV and ITO nanodome TPV taken during the illumination of the light source. Though both devices were prepared under identical conditions and were illuminated with the same intensities of light, yet ITO nanodomes based device showed enhanced generation of photocarriers. Under identical I-V conditions measurements, the improved performance of ITO nanodomes device can be attributed to the focusing of incident light over SCR region. The in-built electric field in the SCR sweeps the photogenerated carrier more efficiently leading high photocurrent under identical illumination conditions [51]. To further investigate the transient photoresponse behavior of both the devices, I-t spectra were also recorded under the illumination of the light source of the wavelength of 365 nm with various power intensities (Fig. 4). The intensity of the light source was varied from 1 to 3.8 mA/cm^2. The chopping frequency of the light source was 70 Hz. Under the illumination of the light of 365 nm, the ITO nanodomes based TPV has shown a significant enhancement in the photocurrent while glass-based TPV demonstrated poor performance (Fig. 4(a) and 4(b)). Since photocurrent depends on the power intensity of the illuminated light source, therefore an enhancement in the photocurrent with the increase in the intensity of illuminated light can be due to the generation of more photocarriers [53, 54].

Under the illumination of the light of 365 nm of power intensity 3.8 mW/cm^2, the ITO nanodome based device exhibited ~1.7 times increase in photocurrent. Both the devices also acted as an efficient spectral transparent photodetector. The incident photon to current efficiency (IPCE) of both the devices was also calculated and shown in Fig. 5 (a). Both the devices demonstrated high spectra selectivity and high IPCE value in the UV region due to the wide band gap characteristics of the TiO_2 and NiO thin films. ITO nanodome substrate-based device exhibited approximately two times higher IPCE compared to the glass substrate-based TPV. At the wavelength of 365 nm, the IPCE was ~11% and ~6% for ITO nanodome based device and glass-based device, respectively. It is worth mentioning that the ITO nanodome based device demonstrated better IPCE over the entire detecting spectra indicating better light-detecting performance. Other photon detection parameters such as responsivity and detectivity were also calculated for different power intensities and shown in Fig. 5(b) and 5(c), respectively. The responsivity and detectivity were calculated by using equation:

$$R = \frac{I_{sc}\left(\frac{mA}{Cm2}\right)}{P\left(\frac{mW}{cm2}\right)} \tag{2}$$

$$D = \frac{R}{\sqrt{2qI_d}} \tag{3}$$

Where R, I_{sc}, P, D, q, and I_d are the responsivity, photocurrent, power density, detectivity, elementary charge, and dark current, respectively. The ITO nanodome based TPV has exhibited greater responsivity and detectivity for different wavelengths. The responsivity and detectivity calculated for the ITO nanodomes based device were 28 mA/W and 7.58 × 10^{10} Jones, respectively. These values indicate the enhancement of 40 % in responsivity and 1509% in detectivity compared to the glass substrate based TPV.

To have more insight into the speed of light detection, rise and fall time were also calculated. Fig. 5(d) shows the I-t response under the illumination of 365 nm of power density 3.8 mW/cm^2. The rise time can be defined as the time taken by the device to increase photocurrent from 10 % to 90 % of its maximum value. Similarly, fall time can be defined by the time taken by the device to decay photocurrent from 90 % to the 10 % of its maximum value. All the measurements were carried out at zero bias conditions. The ITO nanodome based device demonstrated great response speed as compared to the glass substrate-based device. The rise time is reduced from 1.4 ms to 0.31 ms and fall time is reduced from 1.8 ms to 0.32 ms (Fig. 5(e) and 5(f)). The reduction in response time and enhancement in responsivity, detectivity, and IPCE, all are related to the photocurrent. Table 1 summarizes the improved performance of the self-powered NiO/TiO_2/ nanodomes based UV

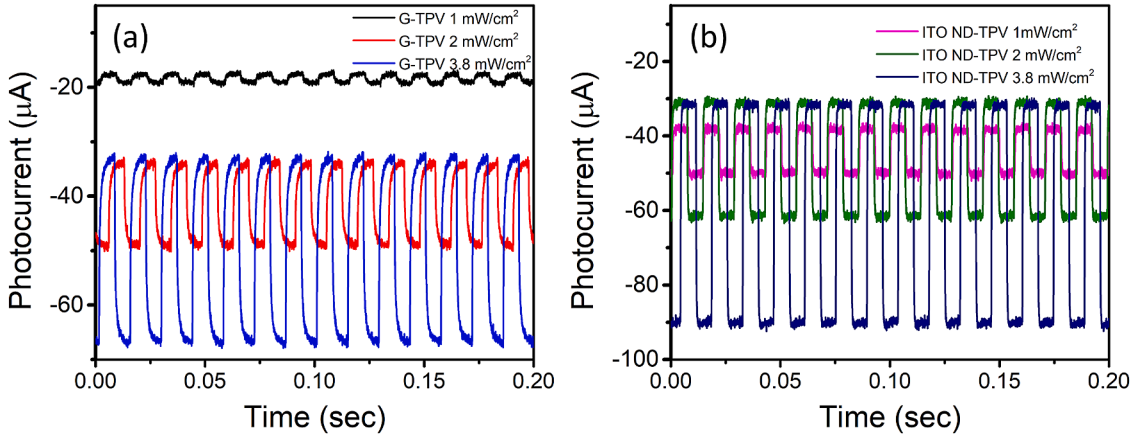

Fig. 4. (a), and (b) are the transient photocurrent response for various intensities with time for glass based TiO_2 /NiO TPV and ITO nanodome based TPV, respectively.

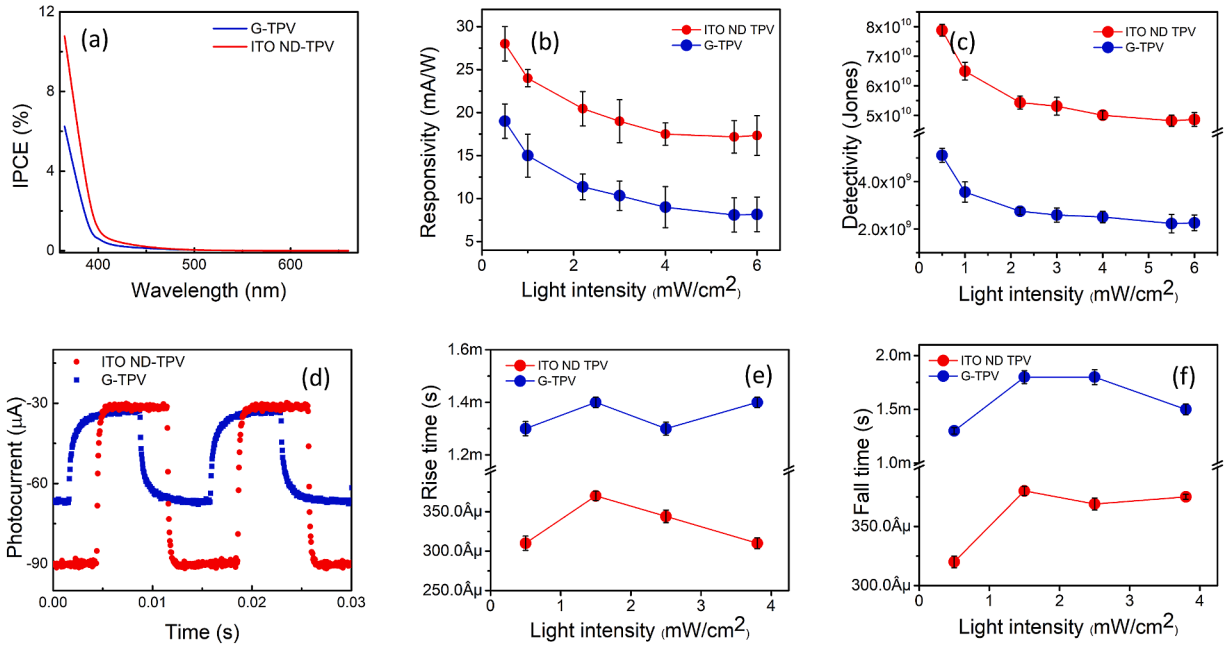

Fig. 5. (a) Incident photon to current efficiency, (b) responsivity, (c) detectivity, (d) I-t response under illumination of 365 nm of power density 3.8 mW/cm^2, (e) rise time and (f) fall time of the glass substrate-based TPV and ITO nanodome based TPV.

Table 1
Comparison of the performance of current, self-powered NiO/TiO_2/Nanodomes UV photodetector with previously reported UV photodetectors.

Device structure	λ(nm)	Bias (V)	R (A/W)	Detectivity (Jones)	Rise time (s)	Fall time (s)	Year; Reference
Au/ZnO/TiO_2/FTO glass	380	6	150	_	0.18	6.63	2015 [56]
Ni/TiO_2/MgF_2	300	5	4.85		43	10	2016 [57]
Cu/TiO_2/FTO glass	365	-1	0.897	4.5×10^{12}	1.12×10^{-3}	1.46×10^{-3}	2017 [58]
NiO/ZnO NW/AZO/ITO glass	380	0	0.0014	_	<0.04	<0.04	2017 [59]
ZnO NWs/FTO glass	365	5	113	_	23	73	2018 [60]
AgNw/ZnO NF/SiO_2/Si	365	0	0.0094	1.7×10^{11}	<1	<1	2019 [61]
Au/TiO/Au	365	4	2.0×10^{-4}	_	0.98	3.14	2019 [62]
Au/TiO_2/graphene oxide/Si	380	3	0.048	2.3×10^{11}	48	40	2019 [63]
FTO/ZnO QD /glass	365	3.6	21.6	_	1.9	51.1	2020 [64]
TiO_2-rGO/glass	375	3	2.1	_	0.051	0.058	2020 [65]
AgNw/NiO/TiO_2/ITO nanodomes	365	0	0.028	7.58×10^{10}	3.1×10^{-4}	3.2×10^{-4}	2021 This work

photodetector over previously reported UV photodetectors. It clearly shows the high responsivity of NiO/TiO_2/ nanodomes device at 0 V with very fast response to the UV light. The enhancement in the responsivity of ITO nanodomes device can be attributed to the increase in photocurrent under the illumination of the light source due to the concentration of incident light over the space charge region. Since high detection of the light depends on the efficient generation of photo carrier, therefore, high photocurrent generation would lead to the high responsivity and high detectivity [55].The photogenerated carriers immediately move away from the space region to respective electrodes, due to the strong built-in electric field inside the space charge region. As the result, significant response time enhancement is observed for ITO nanodome based device.

Mechanism of focusing of incident light and Energy band-diagram

To understand the enhancement in photocurrent generation a fundamental approach of optics of lenses is taken into consideration. The focusing of the incident light at the focal point by the convex and concave lens is illustrated in Fig. 6. Fig. 6(a) and 6(b) show the convergence of the incident light at focal point and divergence of incident light, respectively. Herein, ITO nanodomes acted as a convex lens to converge the light at its focal point. The modeling of the TiO_2/NiO TPV was done in such a way so that the space charge region of TiO_2/NiO lies at the focal length of the ITO nanodome. Though, in the case of nanostructures, calculating focal length takes a diverse approach. The focal length of nanodome was calculated by taking care of several parameters such as height and curvature of nanodomes, the thickness of the films used for TPV fabrication, and refractive indices of the different layers (Table 2).

The radius of curvature was calculated using Eq. (1). The height and radius of the nanodome were 201.25±1.29 nm and 180±0.70 nm, respectively. Then it was needed to calculate the focal length of the ITO nanodome in the air and it was calculated using the following equation:

$$F_{air} = \frac{R}{n_{ITO} - n_{air}} \tag{4}$$

Where n_{ITO} and n_{air} are the refractive index of ITO and air, respectively. Since SCR forms across the junction of TiO_2 and NiO and light passes through high refractive index material, TiO_2, the focal length of ITO nanodomes can be calculated as:

$$F_{dome} = F_{air} \times n_{TiO2} \tag{5}$$

Fig. 6(c) picturizes the complete structure of the fabricated TPV and focusing of the incident light over the SCR region.

To indicate the origin of the high photocurrent and photovoltage, a schematic band diagram of the TiO_2/NiO heterojunction fabricated on the ITO Nano domes substrate is given in Fig. 7. Fig. 7(a) and 7(b) are the

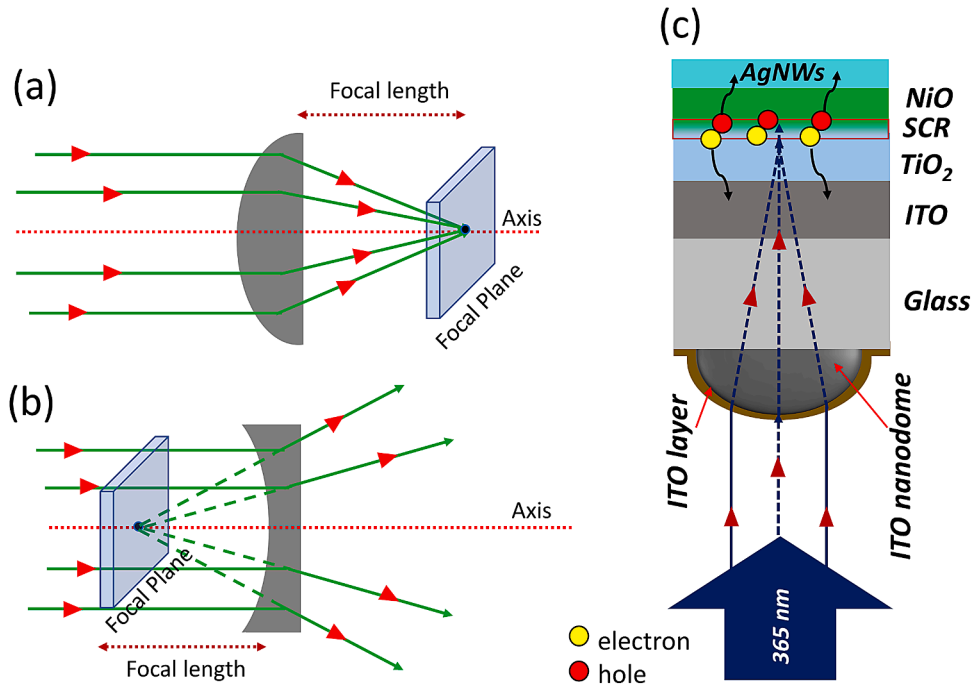

Fig. 6. Basic understanding of focusing of incident light by (a) convex lens and, (b) concave lens. (c) Schematic representation of focusing of light by ITO nanodomes near the space charge region to enhance the generation of photocarrier.

Table 2
Calculation of focal length to determine the thickness of ITO and TiO_2 thin film to focus the light over the SCR region.

λ (nm)	n_{ITO}	F_{air} (nm)	n_{TiO2}	F_{dome} (nm)
365	2.18	153.49±0.60	3.75	575.60±2.26

band diagram of TiO_2/NiO TPV fabricated on the glass substrate and the ITO nanodomes substrate, respectively. Fig. 7(a) shows the absorbance of unfocused light in the TiO_2 material. On the contrary, Fig. 7(b) shows the absorbance and focus of incident light over SCR. By using the ITO nanodome structure and suitable modeling of the TiO_2/NiO device, the incident light can be focused over the SCR region. By focusing the light over the SCR, the overlapping of the photo carrier generation region and the SCR can be achieved. There exists a strong built-in electric field in the SCR that efficiently separates the photogenerated carrier giving high photocurrent and photovoltage. The built-in potential was created by the differences in the Fermi level of TiO_2 and NiO. The TiO_2 and NiO formed a type-II heterostructure, with a cliff that facilitated the electron transfer from the NiO to TiO_2.

Several reports are found where nanostructures such as nanosphere and nanorods were used to magnify and focus the light using the localized surface plasmon resonance [35, 36]. Therefore, this work provides a direct approach to focus the light over SCR for better charge collection efficiency in photovoltaics and improved performance of the UV photodetector without using any other metallic nanostructure integration approach.

Conclusions

A novel and efficient method was demonstrated to improve the photocurrent and photovoltage in TiO_2/NiO TPV by using a periodic nanostructured ITO nanodome substrate. A fundamental approach of optics of lenses was used to focus the light over high electric field region (SCR). The TPV was modeled in such a way that the photo carrier generation region and SCR overlaps for enhanced photogenerated

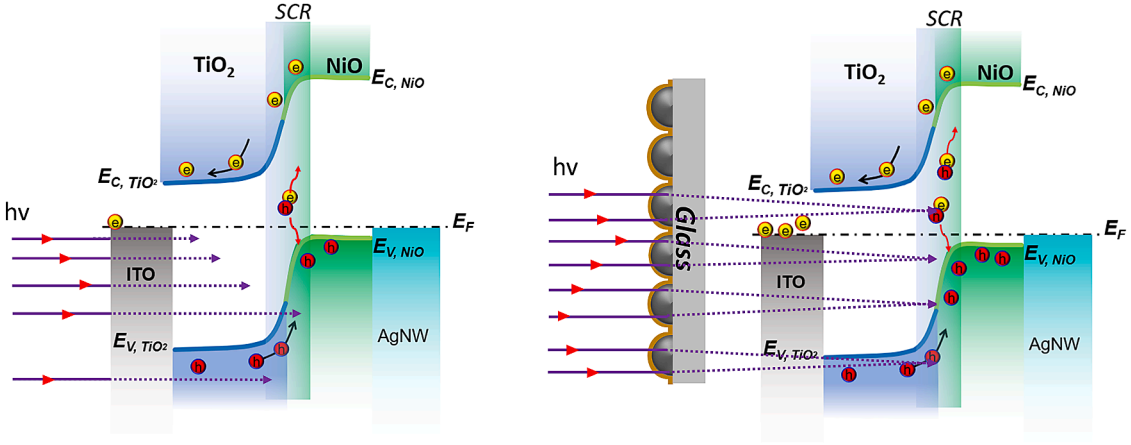

Fig. 7. Schematic band diagram of (a) glass/ITO based TiO_2/NiO transparent photovoltaic and (b) ITO nanodome based TiO_2/NiO transparent photovoltaic.

charge carrier collection efficiency. A significant improvement in the photocurrent (~3 times) and photovoltage (~10 times) was recorded for ITO nanodomes based TiO_2/NiO device compared to TiO_2/NiO TPV fabricate on glass. ITO nanodome substrate-based device also showed a remarkable spectral selectivity in the UV region with high responsivity (28±2 mA/W) and high response speed (<0.5 ms) under self-biasness. Hence, this work provided a simplest and easiest approach to improve the photocurrent and photovoltage that can be benefactors for photovoltaics domain.

Credit author statement

Formal analysis: Naveen Kumar and Thanh Tai Nguyen,
Resources: Joondong Kim and Hyungho Park,
Data Curation: Naveen Kumar, Thanh Tai Nguyen, Sang Moon Kim and Hyungho Park,
Investigation: Joondong Kim and Sang Moon Kim,
Writing - Original Draft: Naveen Kumar and Thanh Tai Nguyen,
Writing - Review & Editing: Naveen Kumar and Joondong Kim,
Funding acquisition: Joondong Kim

Declaration of Competing Interest

The authors declare that they have no known competing financial interests or personal relationships that could have appeared to influence the work reported in this paper.

Acknowledgments

The authors acknowledge the financial support from the Incheon National University (2020-0089), Korea (Republic of) and Basic Science Research Program through the National Research Foundation (NRF-2020R1A2C1009480) by the Ministry of Education of Korea (Republic of).

References

[1] G.R. Adams, O.I. Okoli, A review of Perovskite solar cells with a focus on wire-shaped devices, Renew. Energy Focus 25 (2018) 17–23, https://doi.org/10.1016/j.ref.2018.02.002.
[2] V. Vega-Garita, L. Ramirez-Elizondo, N. Narayan, P. Bauer, Integrating a photovoltaic storage system in one device: a critical review, Prog. Photovolt. 27 (2019) 346–370, https://doi.org/10.1002/pip.3093.
[3] J.N. Bullock, C. Bechinger, D.K. Benson, H.M. Branz, Semi-transparent a-SiC:H solar cells for self-powered photovoltaic-electrochromic devices, J. Non Cryst. Solids 198-200 (1996) 1163–1167, https://doi.org/10.1016/0022-3093(96)00105-6.
[4] W. Jung, T. Hong, J. Oh, H. Kang, M. Lee, Development of a prototype for multi-function smart window by integrating photovoltaic blinds and ventilation system, Build. Environ. 149 (2019) 366–378, https://doi.org/10.1016/j.buildenv.2018.12.026.
[5] M. Yamaguchi, T. Masuda, K. Araki, D. Sato, K.-H. Lee, N. Kojima, T. Takamoto, K. Okumura, A. Satou, K. Yamada, T. Nakado, Y. Zushi, Y. Ohshita, M. Yamazaki, Development of high-efficiency and low-cost solar cells for PV-powered vehicles application, Prog. Photovolt., n/a, 10.1002/pip.3343.
[6] K. Sasaki, M. Yokota, H. Nagayoshi, K. Kamisako, Evaluation of electric motor and gasoline engine hybrid car using solar cells, Sol. Energy Mater. Sol. Cells 47 (1997) 259–263, https://doi.org/10.1016/S0927-0248(97)00047-0.
[7] R. Tipnis, J. Bernkopf, S. Jia, J. Krieg, S. Li, M. Storch, D. Laird, Large-area organic photovoltaic module—Fabrication and performance, Sol. Energy Mater. Sol. Cells 93 (2009) 442–446, https://doi.org/10.1016/j.solmat.2008.11.018.
[8] P.K. Nayak, S. Mahesh, H.J. Snaith, D. Cahen, Photovoltaic solar cell technologies: analysing the state of the art, Nat. Rev. Mater. 4 (2019) 269–285, https://doi.org/10.1038/s41578-019-0097-0.
[9] M. Riede, D. Spoltore, K. Leo, Organic solar cells—the path to commercial success, Adv. Energy Mater. 11 (2021), 2002653, https://doi.org/10.1002/aenm.202002653.
[10] S.H. Park, S. Park, S. Lee, J. Kim, H. Ahn, B.J. Kim, B. Chae, H.J. Son, Developement of highly efficient large area organic photovoltaic module: Effects of nonfullerene acceptor, Nano Energy 77 (2020), 105147, https://doi.org/10.1016/j.nanoen.2020.105147.
[11] N. Li, X. Niu, Q. Chen, H. Zhou, Towards commercialization: the operational stability of Perovskite solar cells, Chem. Soc. Rev. 49 (2020) 8235–8286, https://doi.org/10.1039/D0CS00573H.
[12] L. Qiu, L.K. Ono, Y. Qi, Advances and challenges to the commercialization of organic–inorganic halide Perovskite solar cell technology, Mater. Today Energy 7 (2018) 169–189, https://doi.org/10.1016/j.mtener.2017.09.008.
[13] K. Lee, H.-D. Um, D. Choi, J. Park, N. Kim, H. Kim, K. Seo, The development of transparent photovoltaics, Cell Rep. Phys. Sci. 1 (2020), 100143, https://doi.org/10.1016/j.xcrp.2020.100143.
[14] P. Heinstein, C. Ballif, L.-E. Perret-Aebi, Building Integrated Photovoltaics (BIPV): review, potentials, barriers and myths, Green, 3 (2013) 125-156, 10.1515/green-2013-0020.
[15] T. Soga, Chapter 1 - fundamentals of solar cell, in: T. Soga (Ed.), Nanostructured Materials for Solar Energy Conversion, Elsevier, Amsterdam, 2006, pp. 3–43.
[16] S.-Y. Chang, P. Cheng, G. Li, Y. Yang, Transparent polymer photovoltaics for solar energy harvesting and beyond, Joule 2 (2018) 1039–1054, https://doi.org/10.1016/j.joule.2018.04.005.
[17] H. Zhang, Y. Li, X. Zhang, Y. Zhang, H. Zhou, Role of interface properties in organic solar cells: from substrate engineering to bulk-heterojunction interfacial morphology, Mater. Chem. Front. 4 (2020) 2863–2880, https://doi.org/10.1039/D0QM00398K.
[18] T. Chen, W. Hu, J. Song, G.H. Guai, C.M. Li, Interface functionalization of photoelectrodes with graphene for high performance dye-sensitized solar cells, Adv. Funct. Mater. 22 (2012) 5245–5250, https://doi.org/10.1002/adfm.201201126.
[19] D. Gaspar, L. Pereira, K. Gehrke, B. Galler, E. Fortunato, R. Martins, High mobility hydrogenated zinc oxide thin films, Sol. Energy Mater. Sol. Cells 163 (2017) 255–262, https://doi.org/10.1016/j.solmat.2017.01.030.
[20] S. Parthiban, V. Gokulakrishnan, K. Ramamurthi, E. Elangovan, R. Martins, E. Fortunato, R. Ganesan, High near-infrared transparent molybdenum-doped indium oxide thin films for nanocrystalline silicon solar cell applications, Sol. Energy Mater. Sol. Cells 93 (2009) 92–97, https://doi.org/10.1016/j.solmat.2008.08.007.
[21] L.C.-K. Liau, J.-S. Huang, Effect of indium- and gallium-doped ZnO fabricated through sol-gel processing on energy level variations, Mater. Res. Bull. 97 (2018) 6–12, https://doi.org/10.1016/j.materresbull.2017.08.044.
[22] J. Xie, C. Guo, C.M. Li, Interface functionalization with polymer self-assembly to boost photovoltage of Cu_2O/ZnO nanowires solar cells, Int. J. Hydrog. Energy 39 (2014) 16227–16233, https://doi.org/10.1016/j.ijhydene.2014.04.108.
[23] N.K. Elumalai, C. Vijila, R. Jose, A. Uddin, S. Ramakrishna, Metal oxide semiconducting interfacial layers for photovoltaic and photocatalytic applications, Mater. Renew. Sustain. Energy 4 (2015) 11, https://doi.org/10.1007/s40243-015-0054-9.
[24] F. Han, Z. Tu, Z. Wan, J. Luo, J. Xia, G. Hao, Y. Yi, R. Wang, C. Jia, Effect of functional group position change of pyridinesulfonic acid as interface-modified layer on perovskite solar cell, App. Surf. Sci. 462 (2018) 517–525, https://doi.org/10.1016/j.apsusc.2018.08.088.
[25] A. Mavrokefalos, S.E. Han, S. Yerci, M.S. Branham, G. Chen, Efficient light trapping in inverted nanopyramid thin crystalline silicon membranes for solar cell applications, Nano Lett 12 (2012) 2792–2796, https://doi.org/10.1021/nl2045777.
[26] M.M. Adachi, M.P. Anantram, K.S. Karim, Core-shell silicon nanowire solar cells, Sci. Rep. 3 (2013) 1546, https://doi.org/10.1038/srep01546.
[27] K.X. Wang, Z. Yu, V. Liu, Y. Cui, S. Fan, Absorption enhancement in ultrathin crystalline silicon solar cells with antireflection and light-trapping nanocone gratings, Nano Lett 12 (2012) 1616–1619, https://doi.org/10.1021/nl204550q.
[28] J.B. Orhan, R. Monnard, E. Vallat-Sauvain, L. Fesquet, D. Romang, X. Multone, J. F. Boucher, J. Steinhauser, D. Dominé, J.P. Cardoso, D. Borrello, G. Charitat, B. Dehbozorgi, G. Choong, M. Charrière, S. Benagli, J. Meier, J. Bailat, J. Escarré, N. Blondiaux, J. Sakurai, J. Lin, A. Matsunaga, P. Losio, Nano-textured superstrates for thin film silicon solar cells: Status and industrial challenges, Sol. Energy Mater. Sol. Cells 140 (2015) 344–350, https://doi.org/10.1016/j.solmat.2015.04.027.
[29] F. Priolo, T. Gregorkiewicz, M. Galli, T.F. Krauss, Silicon nanostructures for photonics and photovoltaics, Nat. Nanotechnol. 9 (2014) 19–32, https://doi.org/10.1038/nnano.2013.271.
[30] K. Seo, Y.J. Yu, P. Duane, W. Zhu, H. Park, M. Wober, K.B. Crozier, Si microwire solar cells: improved efficiency with a conformal SiO_2 layer, ACS Nano 7 (2013) 5539–5545, https://doi.org/10.1021/nn401776x.
[31] B. Tian, X. Zheng, T.J. Kempa, Y. Fang, N. Yu, G. Yu, J. Huang, C.M. Lieber, Coaxial silicon nanowires as solar cells and nanoelectronic power sources, Nature 449 (2007) 885–889, https://doi.org/10.1038/nature06181.
[32] E. Fortunato, P. Nunes, A. Marques, D. Costa, H. Águas, I. Ferreira, M.E.V. Costa, M.H. Godinho, P.L. Almeida, J.P. Borges, R. Martins, Transparent, conductive ZnO: Al thin film deposited on polymer substrates by RF magnetron sputtering, Surf. Coat. Tech. 151-152 (2002) 247–251, https://doi.org/10.1016/S0257-8972(01)01660-7.
[33] S. Ullah, R. Branquinho, T. Mateus, R. Martins, E. Fortunato, T. Rasheed, F. Sher, Solution combustion synthesis of transparent conducting thin films for sustainable photovoltaic applications, Sustainability 12 (2020) 10423.
[34] E. Muchuweni, T.S. Sathiaraj, H. Nyakotyo, Effect of O_2/Ar flow ratio on Ga and Al co-doped ZnO thin films by rf sputtering for optoelectronic device fabrication, Mater. Res. Bull. 95 (2017) 123–128, https://doi.org/10.1016/j.materresbull.2017.07.029.
[35] K. Li, M.I. Stockman, D.J. Bergman, Self-similar chain of metal nanospheres as an efficient nanolens, Phys. Rev. Lett. 91 (2003), 227402, https://doi.org/10.1103/PhysRevLett.91.227402.
[36] S. Kawata, A. Ono, P. Verma, Subwavelength colour imaging with a metallic nanolens, Nat. Photonics 2 (2008) 438–442, https://doi.org/10.1038/nphoton.2008.103.

[37] M.h. Mohammadi, M. Eskandari, D. Fathi, Effects of the location and size of plasmonic nanoparticles (Ag and Au) in improving the optical absorption and efficiency of perovskite solar cells, J. Alloys Compd. 877 (2021), 160177, https://doi.org/10.1016/j.jallcom.2021.160177.
[38] J. Xue, J. Liu, S. Mao, Y. Wang, W. Shen, W. Wang, L. Huang, H. Li, J. Tang, Recent progress in synthetic methods and applications in solar cells of Ag2S quantum dots, Mater. Res. Bull. 106 (2018) 113–123, https://doi.org/10.1016/j.materresbull.2018.05.041.
[39] Z. Ge, C. Wang, Z. Chen, T. Wang, T. Chen, R. Shi, S. Yu, J. Liu, Investigation of the TiO_2 nanoparticles aggregation with high light harvesting for high-efficiency dye-sensitized solar cells, Mater. Res. Bull. 135 (2021), 111148, https://doi.org/10.1016/j.materresbull.2020.111148.
[40] K.B. Bhojanaa, M. Ramesh, A. Pandikumar, Complementary properties of silver nanoparticles on the photovoltaic performance of titania nanospheres based photoanode in dye-sensitized solar cells, Mater. Res. Bull. 122 (2020), 110672, https://doi.org/10.1016/j.materresbull.2019.110672.
[41] P.K. Jain, Taking the heat off of plasmonic chemistry, J. Phys. Chem. C 123 (2019) 24347–24351, https://doi.org/10.1021/acs.jpcc.9b08143.
[42] E.C. Garnett, B. Ehrler, A. Polman, E. Alarcon-Llado, Photonics for photovoltaics: advances and opportunities, ACS Photonics 8 (2021) 61–70, https://doi.org/10.1021/acsphotonics.0c01045.
[43] J. Peoples, X. Li, Y. Lv, J. Qiu, Z. Huang, X. Ruan, A strategy of hierarchical particle sizes in nanoparticle composite for enhancing solar reflection, Int. J. Heat Mass Transf. 131 (2019) 487–494, https://doi.org/10.1016/j.ijheatmasstransfer.2018.11.059.
[44] J.W. Lim, G. Kim, M. Shin, S.J. Yun, Colored a-Si:H transparent solar cells employing ultrathin transparent multi-layered electrodes, Sol. Energy Mater. Sol. Cells 163 (2017) 164–169, https://doi.org/10.1016/j.solmat.2017.01.017.
[45] A. Mutalikdesai, S.K. Ramasesha, Solution process for fabrication of thin film CdS/CdTe photovoltaic cell for building integration, Thin Solid Films 632 (2017) 73–78, https://doi.org/10.1016/j.tsf.2017.04.036.
[46] G. Xu, L. Shen, C. Cui, S. Wen, R. Xue, W. Chen, H. Chen, J. Zhang, H. Li, Y. Li, Y. Li, High-performance colorful semitransparent polymer solar cells with ultrathin hybrid-metal electrodes and fine-tuned dielectric mirrors, Adv. Funct. Mater. 27 (2017), 1605908, https://doi.org/10.1002/adfm.201605908.
[47] H.-C. Kwon, A. Kim, H. Lee, D. Lee, S. Jeong, J. Moon, Parallelized nanopillar perovskites for semitransparent solar cells using an anodized aluminum oxide scaffold, Adv. Energy Mater. 6 (2016), 1601055, https://doi.org/10.1002/aenm.201601055.
[48] M. Pavan, S. Rühle, A. Ginsburg, D.A. Keller, H.-N. Barad, P.M. Sberna, D. Nunes, R. Martins, A.Y. Anderson, A. Zaban, E. Fortunato, TiO_2/Cu_2O all-oxide heterojunction solar cells produced by spray pyrolysis, Sol. Energy Mater. Sol. Cells 132 (2015) 549–556, https://doi.org/10.1016/j.solmat.2014.10.005.
[49] T.T. Nguyen, M. Patel, S. Kim, R.A. Mir, J. Yi, V.-A. Dao, J. Kim, Transparent photovoltaic cells and self-powered photodetectors by TiO_2/NiO heterojunction, J. Power Sources 481 (2021), 228865, https://doi.org/10.1016/j.jpowsour.2020.228865.
[50] K. Nakayama, C. Luangchaisri, C. Muangphat, K. Praweerawat, Preparation of NiO/TiO2 composite films for enhanced dye sensitized solar cell efficiency, Mater. Today: Proc., 23 (2020) 690-695, 10.1016/j.matpr.2019.12.260.
[51] J.-H. Yun, E. Lee, H.-H. Park, D.-W. Kim, W.A. Anderson, J. Kim, N.M. Litchinitser, J. Zeng, J. Yi, M.M.D. Kumar, J. Sun, Incident light adjustable solar cell by periodic nanolens architecture, Sci. Rep. 4 (2014) 6879, https://doi.org/10.1038/srep06879.
[52] C.M. Proctor, T.-Q. Nguyen, Effect of leakage current and shunt resistance on the light intensity dependence of organic solar cells, App. Phys. Lett. 106 (2015), 083301, https://doi.org/10.1063/1.4913589.
[53] Q. Zhao, W. Wang, F. Carrascoso-Plana, W. Jie, T. Wang, A. Castellanos-Gomez, R. Frisenda, The role of traps in the photocurrent generation mechanism in thin InSe photodetectors, Mater. Horiz. 7 (2020) 252–262, https://doi.org/10.1039/C9MH01020C.
[54] Single-crystalline ZnTe nanowires for application as high-performance Green/Ultraviolet photodetector, Opt. Express 19 (2011) 6100–6108, https://doi.org/10.1364/OE.19.006100.
[55] A.T. Vicente, A. Araújo, M.J. Mendes, D. Nunes, M.J. Oliveira, O. Sanchez-Sobrado, M.P. Ferreira, H. Águas, E. Fortunato, R. Martins, Multifunctional cellulose-paper for light harvesting and smart sensing applications, J. Mater. Chem. C 6 (2018) 3143–3181, https://doi.org/10.1039/C7TC05271E.
[56] D. Zhang, X. Gu, F. Jing, F. Gao, J. Zhou, S. Ruan, High performance ultraviolet detector based on TiO_2/ZnO heterojunction, J. Alloys Compd. 618 (2015) 551–554, https://doi.org/10.1016/j.jallcom.2014.09.004.
[57] Y. Xie, L. Wei, Q. Li, Y. Chen, S. Yan, J. Jiao, G. Liu, L. Mei, Epitaxial rutile TiO_2 film based on MgF_2 substrate for ultraviolet detector, J. Alloys Compd. 683 (2016) 439–443, https://doi.org/10.1016/j.jallcom.2016.05.126.
[58] D.B. Patel, K.R. Chauhan, W.-H. Park, H.-S. Kim, J. Kim, J.-H. Yun, Tunable TiO_2 films for high-performing transparent Schottky photodetector, Mater. Sci. Semicond. Process. 61 (2017) 45–49, https://doi.org/10.1016/j.mssp.2016.12.036.
[59] Z. Chen, B. Li, X. Mo, S. Li, J. Wen, H. Lei, Z. Zhu, G. Yang, P. Gui, F. Yao, G. Fang, Self-powered narrowband p-NiO/n-ZnO nanowire ultraviolet photodetector with interface modification of Al_2O_3, App. Phys. Lett. 110 (2017), 123504, https://doi.org/10.1063/1.4978765.
[60] L. Yin, H. Ding, Z. Yuan, W. Huang, C. Shuai, Z. Xiong, J. Deng, T. Lv, A simple and transparent well-aligned ZnO nanowire array ultraviolet photodetector with high responsivity, Opt. Mater. 80 (2018) 149–153, https://doi.org/10.1016/j.optmat.2018.04.047.
[61] M. Kumar, H. Jeong, D. Lee, UV photodetector with ZnO nanoflowers as an active layer and a network of Ag nanowires as transparent electrodes, Superlattices Microstruct 126 (2019) 132–138, https://doi.org/10.1016/j.spmi.2018.12.004.
[62] P. Gu, X. Zhu, H. Wu, J. Li, D. Yang, Influence of oxygen vacancy on the response properties of TiO_2 ultraviolet detectors, J. Alloys Compd. 779 (2019) 821–830, https://doi.org/10.1016/j.jallcom.2018.11.283.
[63] P. Deb, J.C. Dhar, Fast response UV photodetection using TiO_2 nanowire/graphene oxide thin-film heterostructure, IEEE Photon. Technol. Lett. 31 (2019) 571–574, https://doi.org/10.1109/LPT.2019.2900283.
[64] Z. Yuan, W. Wang, H. Wu, F. Nie, J. He, A solution-processed ZnO quantum dots ultraviolet photodetector with high performance driven by low operating voltage, Mater. Lett. 278 (2020), 128413, https://doi.org/10.1016/j.matlet.2020.128413.
[65] A.S. AlShammari, M.M. Halim, F.K. Yam, N.H.M. Kaus, Effect of precursor concentration on the performance of UV photodetector using TiO_2/reduced graphene oxide (rGO) nanocomposite, Results Phys 19 (2020), 103630, https://doi.org/10.1016/j.rinp.2020.103630.